TOTAL HEMISPHERICAL EMISSIVITY OF OXIDIZED INCONEL 718 IN THE TEMPERATURE RANGE 300°C TO 1000°C

G.A. Greene and C.C. Finfrock
Brookhaven National Laboratory
Upton, New York 11973-5000

and

T.F. Irvine, Jr.
State University of New York at Stony Brook
Stony Brook, New York 11794-2300

April 2000

ABSTRACT

Total hemispherical emissivities were measured for Inconel 718 as a function of sample temperature. Measurements were made with both unoxidized and oxidized samples. The oxidation temperatures were 1000°C, 1100°C and 1142°C and the oxidation times were 15, 30 and 60 minutes. The oxidized samples showed a significant increase in emissivity over the unoxidized one which was in an as received condition. No apparent pattern was observed in the change of emissivity as a function of oxidation time at a given oxidation temperature. In some cases, emissivity measurements made with increasing temperature were greater than those made with descending temperature. One possible explanation for this is the spalling of the oxide layer as the sample area contracted with descending sample temperature.

Address all correspondence to:
Dr. George Greene
Brookhaven National Laboratory
Building 820M
Upton, NY 11973-5000
631-344-2296 (voice)
631-344-3526 (fax)
greene@bnl.gov

Under contract number DE-AC02-98CH10886 with the United States Department of Energy

1. INTRODUCTION

Heat transfer in high vacuum systems occurs primarily by thermal radiation. In order to calculate such radiation transfers, it is necessary to know the radiation properties of the surfaces which are emitting and absorbing radiation. In general, these properties must be determined experimentally and the surface properties of the test materials must be as close as possible to those under actual operating conditions.

Unfortunately, such measurements are not always simple to accomplish, particularly when the surface properties change with time as is often the case. Thus, one must make radiation property measurements over a range of surface conditions to attempt to bracket these property values and to better understand their influence on the radiation heat transfer processes.

The present investigation considers thermal radiation heat transfer under vacuum conditions where the radiating and absorbing surfaces are Inconel 718. The purpose for this research was to develop highly precise data of the total hemispherical emissivity of oxidized Inconel 718 for application to the analyses of accident conditions in proton spallation targets under conditions in which the target clad material is simultaneously oxidized and overheated to high temperatures. The crucial parameter in calculating the peak temperatures of such targets during thermal transients is the radiative emissivity of the Inconel 718 clad. Radiation heat transfer calculations can only be as accurate and precise as the values of the radiative emissivity that go into the calculations; using emissivities which are either too low or too high will drive the calculated peak temperatures to extremes which renders parametric calculations of little value. Best-estimate accident calculations require precise and accurate thermal

radiative emissivity data. A search of the literature failed to find any previous measurements of the radiation properties of this material precise enough for the present application [1-3]. Of particular interest are the effects of surface oxidation and temperature on the emissivity. Therefore, the present investigation was conducted, the purpose of which was the measurement of total hemispherical emissivities over a range of temperatures (200°C T 1000°C) and a variety of surface oxidation conditions.

The above discussion can be illustrated by reference to Fig. 1 from [3]. In the figure are measured total hemispherical emissivities under a variety of surface and temperature conditions. It is seen first of all that the emissivities increase with temperature under all surface conditions. In addition, curve A whose surface is in the as rolled condition has the lowest emissivity of the three samples. Curve B which is in the as rolled condition but which has been oxidized in air at a temperature of 815°C for 15 minutes has a significantly larger emissivity than curve A. Finally, curve C which has been sand blasted to increase its surface roughness and also oxidized has the largest emissivities of all three samples. That these differences are significant is illustrated by the figure where at 400°C, the thermal radiation emitted by surface C is more than 2.5 times the radiation of surface A.

2. THEORY

Figure 2 illustrates the basic theory of the experimental apparatus. If A_1 is the experimental sample and A_2 represents the surroundings, then the radiosity J is related to the blackbody emissive power E_b and the irradiation of surface A_1 by G as follows,

$$J_1 = \epsilon_1 E_{b1} + \rho_1 G_1 \qquad (1)$$

Since $\rho_1 = (1 - \alpha_1)$ and if the surface A_1 is opaque and the system is either gray or close enough to thermal equilibrium so that $\alpha = \epsilon$, then Eq. (1) becomes,

$$J_1 = \epsilon_1 E_{b1} + (1 - \epsilon_1) G_1 \qquad \text{or,} \qquad (2)$$

$$G_1 = \frac{J_1 - \epsilon_1 E_{b1}}{(1 - \epsilon_1)}$$

However, the net heat flow from surface A_1 is the difference between the radiosity and irradiation.

$$\frac{Q_1}{A_1} = J_1 - G_1 \qquad (3)$$

Combining Eqs. (2) and (3) yields the following for the surface heat flux from A_1,

$$Q_1 = \frac{E_{b1} - J_1}{(1 - \epsilon_1)/A_1 \epsilon_1} \qquad (4)$$

A similar relationship may be developed for surface A_2 by the same methodology. The denominator of Eq. (4) can be considered a surface resistance to heat transfer. Consider now the exchange of

radiant energy between two surfaces A_1 and A_2. The total radiation which leaves surface 1 and reaches surface 2 is $J_1 A_1 F_{12}$, and the total energy which leaves surface 2 and reaches surface 1 is $J_2 A_2 F_{21}$. Thus, the net radiant energy interchange between the two surfaces in terms of radiosity is $(Q_1 - Q_2) = Q_{1\text{-}2} = (J_1 A_1 F_{12} - J_2 A_2 F_{21})$, where F_{12} is the angle factor between 1 and 2. Since $A_1 F_{12} = A_2 F_{21}$, this relation can be rewritten as follows,

$$Q_{1-2} = \frac{J_1 - J_2}{1/(A_1 F_{12})} = \frac{J_1 - J_2}{1/(A_2 F_{21})} \tag{5}$$

The denominator of Eq. (5) can be considered a spatial resistance to heat transfer. Using Eqs. (4) and (5), one can solve for the overall net heat transfer between surfaces A_1 and A_2 as shown below.

$$Q_{1-2} = \frac{E_{b1} - E_{b2}}{\frac{1-\epsilon_1}{A_1 \epsilon_1} + \frac{1}{A_1 F_{12}} + \frac{1-\epsilon_2}{A_2 \epsilon_2}} \tag{6}$$

However, since $F_{12} = 1$, and $A_1 << A_2$ or $\epsilon_2 = 1$,

$$Q_{1-2} = A_1 \epsilon_1 \sigma (T_1^4 - T_2^4) \tag{7a}$$

or

$$\epsilon_1 = \frac{Q_{1-2}}{A_1 \sigma (T_1^4 - T_2^4)} \qquad (7b)$$

Equation (7b) is the operative equation of the experimental apparatus. It contains the following assumptions:

1. The thermal radiation emitted, absorbed and reflected in the system is diffuse.

2. The area of the sample is small compared to the area of the surroundings. Physically this means that only an insignificant amount of radiation emitted by A_1 returns to A_1 from A_2. Also, if A_2 is black ($\epsilon_2 = 1$) as described below, then Eq. (6) becomes Eq. (7a).

3. Kirchhoff's law holds for the sample ($\alpha_1 = \epsilon_1$) which requires either that T_2 is equal to T_1 or the sample is gray, i.e., ϵ_1 is not a function of the wavelength.

Of all of the above assumptions, the effect of the use of Kirchhoff's law is the most difficult to quantify. Since the incoming radiation is small compared to the radiation from the test sample, it is not absolutely necessary to use Kirchhoff's law as is illustrated in Eq. (2). The discussion that follows will illustrate the maximum errors that can be incurred by neglecting Kirchhoff's law (i.e., by neglecting incoming radiation). If the enclosure radiation on the test sample is neglected, then Eq. (7b) becomes,

$$\epsilon_1 = \frac{Q_{1-2}}{A_1 \sigma T_1^4} \tag{8}$$

Thus, the fractional difference between Eq. (7b) and Eq. (8) is,

$$\frac{\epsilon_{1, \text{Eq. 7b}} - \epsilon_{1, \text{Eq. 8}}}{\epsilon_{1, \text{Eq. 7b}}} = (T_2/T_1)^4 \tag{9}$$

For an enclosure temperature T_2 equal to 300 K, Table 1 lists these differences.

The maximum error incurred by the misuse of Kirchhoff's law (i.e., assuming $\alpha_1 = \epsilon_1$) is bounded by the error incurred by neglecting incoming radiation to the sample altogether. Assuming that the neglect of incoming radiation is an upper bound on any errors occasioned by using Kirchhoff's law ($\alpha_1 = \epsilon_1$), these errors are illustrated in Table 1. For T_1 800 K, this would cause maximum errors of less than 2%. Errors at other temperatures can be estimated from Table 1 or Eq. (9). Also, the measured values of ϵ_1 from Eq. (7b) would be equal to or slightly higher than the actual emissivities, depending on the fidelity of the experiment to the requirements of Kirchhoff's law (i.e., $\alpha_1 = \epsilon_1$). The actual errors are expected to be less than the values in Table 1 over the complete range of T_1. In the lower temperature range, 300 K < T_1 < 500 K, the conditions approach those for which Kirchhoff's law is valid.

3. TEST SAMPLE PREPARATION AND EXPERIMENTAL APPARATUS

Samples were prepared from Inconel 718 alloy material by successively rolling and annealing bar stock to a material thickness of 0.005 inch (0.127 mm). Strips of this material were cut to a rough size of six inches (152.4 mm) long by 0.125 inch (3.175 mm) wide using tin snips. A fixture was designed and fabricated to allow the long edges of the samples to be surface ground parallel and to a uniform width. Final strip widths were nominally 0.105 inch (2.667 mm). Sample thickness and width dimensions were measured with a calibrated micrometer to a precision of ±0.0001 inch (±0.0025 mm). All other dimensions, such as strip heated length and wire positions, were measured with a calibrated dial-indicating caliper to a precision of ±0.0005 inch (±0.0127 mm). Strips were instrumented with type-S (Pt/Pt-10%Rh) thermocouples fabricated from 0.005 inch (0.127 mm) diameter wire. The type-S wires were individually spot welded to the strips by a capacitive discharge technique, spanning the centerline in close proximity to each other. This ensured that the thermocouple junction mass was as small as possible and as closely coupled to the strip as possible. Three thermocouples were attached to each strip with one at the center of the long dimension of the strip, and the other two displaced 0.75 inches (19.05 mm) in either direction. Two 0.005 inch (0.127 mm) diameter Pt wire potential taps were also spot welded to the strips on the strip centerline displaced 0.50 inch (12.7 mm) in either direction from the center thermocouple. Thermocouple and potential tap attachments were made prior to oxidation of the strips to ensure a high quality bond with the substrate. After cleaning with solvents to remove any oils or fingerprints, samples were then oxidized in air to their prescribed conditions in a specially prepared fused quartz fixture. This fixture supported the strip in such a way as to protect the attached leads, and to guarantee that all sides of the strip received uniform exposure to the furnace conditions. Figure 3, a schematic of a sample

whose emissivity is to be measured, illustrates the actual experimental measurement techniques. The sample is heated by passing 60 Hz alternating current, *i*, down the long axis. The voltage drop, ΔV, is measured across the measured sample length, . The sample area of interest is taken as 2 w (the area used in the actual calculations also includes the area contributed by the sample edges). The center temperature is taken as the sample temperature, and the other two measurements made to ensure that the sample is isothermal across . Rewriting Eq. (7b) in terms of the variables in Fig. 3 yields the following expression for the emissivity.

$$\epsilon = \frac{i\ \Delta V}{2\ w\sigma\ (T_1^4 - T_2^4)} \tag{10}$$

The apparatus is illustrated schematically in Fig. 4 and described in detail below. The system was designed and constructed drawing on guidance gained from references [4-7]. A vacuum chamber was fabricated from eight-inch diameter stainless steel tube, seven inches long and painted flat black on its interior. This tube was equipped with eight-inch Conflat flanges on each end. One end was closed with a blank flange and copper gasket. The blank flange formed the floor of the vacuum chamber. Midway up the side of the vessel, a 1.5 inch diameter nipple was welded in radially and equipped with a 1.5 inch Conflat flange for connection to the vacuum system. The upper eight-inch flange carried several vacuum feedthroughs equipped with terminals appropriate for the connection of type-S thermocouples and also connection of the potential taps. The thermocouples were connected by extension grade wire to an ice point cold junction for temperature reference. The center of the upper eight-inch flange incorporated a 1.5 inch Conflat-type machining detail to allow the placement of the

sample holder into the vacuum space. The sample holder was fabricated on the end of a high-current vacuum feedthrough and held the sample on the vertical centerline of the vacuum chamber. A copper fixed-grip was attached to the short leg of the feedthrough, and a spring loaded floating-grip was mounted to the long leg. Upon installation of the sample in the vacuum chamber, care was taken to insure that the sample was rotated such that the sample faces did not view either the 1.5 inch vacuum connection or the long high-current lead. The upper eight-inch flange was sealed with a Viton quad ring gasket to facilitate repeated assembly and disassembly. The chamber was pumped by an oil diffusion pump equipped with a liquid nitrogen cold trap, and backed by a rotary vane mechanical roughing pump. This system routinely achieved a vacuum in the low 10^{-6} Torr range. Power was provided to heat the sample by a high current, low voltage, variable AC transformer. A Hewlett Packard 3455A digital voltmeter and Hewlett Packard scanner were used for all voltage measurements, both AC and DC. Both instruments were controlled and data was acquired via IEEE-488 bus communication to a personal computer. Current was determined by using the above instrumentation to measure the voltage drop across a calibrated multi range selectable precision shunt in series with the sample. Measurements of the three sample thermocouples, the sample voltage drop at the potential taps, the total sample voltage drop, the shunt resistor voltage drop and the vacuum vessel wall temperature were made once every 10 seconds during periods of data acquisition. All data were imported into Excel spreadsheets for analyses. Calculations in the spreadsheets incorporated the current shunt correction factors, calculation of sample surface area based on an individual sample's measurements and thermal expansion effects as a function of temperature.

4. MEASUREMENT ERRORS

Equation (7b), the operative equation of the apparatus, can be utilized to approximately predict the experimental errors of the emissivity measurements. Both $Q_{1\text{-}2}$ and A_1 are implicit functions of other variables as shown in Eq. (10). The RMS uncertainties of the measured emissivities can be computed directly from this equation. The measurements of ΔV and i were the result of measurements of AC voltage with a Hewlett Packard 3455A digital voltmeter; the unit is a five-digit precision voltmeter with calibrated uncertainty of ± (0.04% + 40 digits). The measurement limits of the heat transfer area of the sample (the area bounded by the voltage tap wires) were stipulated previously. The most significant errors in the computation of the emissivity appear in the measurements of the sample and enclosure temperatures themselves, due to conduction of heat along and thermal radiation from the thermocouple wires. Utilizing the heat transfer analysis for a radiating wire [8] and the temperature depression on the sample at the location where the wire is attached [9], the errors in T_1 and T_2 were estimated as shown in Table 2 along with the contributions to the overall error from the other variables. Thus, the overall measurement error of the emissivity as calculated by Eq. (11) below is estimated to be less than 3%.

$$e_\epsilon = \left(\frac{\Delta\epsilon}{\epsilon}\right) = \left[\left(\frac{\Delta i}{i}\right)^2 + \left(\frac{\Delta V}{V}\right)^2 + \left(\frac{\Delta}{}\right)^2 + \left(\frac{\Delta w}{w}\right)^2 + \left(\frac{4\Delta T_1}{T_1}\right)^2 + \left(\frac{4\Delta T_2}{T_2}\right)^2\right]^{1/2} \quad (11)$$

5. EXPERIMENTAL RESULTS AND DISCUSSION

As previously mentioned, the emissivity samples were Inconel 718. Table 3 lists the constituents for this particular alloy. Ten experimental runs were made on Inconel 718 samples under various surface oxidation and surface temperature conditions. Table 4 lists these temperature and oxidation

conditions for nine of the runs (002 and 003 and 005 to 011). Run number 001 was for an unoxidized sample in an as rolled condition from the manufacturer. Run number 004 was an oxidation in a CO_2 atmosphere which is not relevant to the present investigation. The oxidations were carried out within the enclosure at atmospheric pressure by maintaining the surface temperatures for the indicated times.

Figure 10c (which is discussed out of order) illustrates the difficulty encountered in measuring emissivities when the surface temperature exceeded 1000°C. Above this temperature, the thermocouples began to give anomalous readings for unknown causes. This anomaly was investigated further by a separate experiment. In this experiment, a thermocouple was welded to a small piece of Inconel 718 and then wrapped around the standard thermocouple tube. The thermocouples were then placed in a furnace at atmospheric pressure and a comparison was made of the two measured temperatures. The results are shown in Fig. 5 which shows the difference between the two measured temperatures as a function of the measured standard temperature. Under these experimental conditions, an anomaly in the Seebeck coefficient of the spot welded thermocouple can be clearly seen which has a maximum effect at approximately 1000°C. It is believed that the same anomalous condition appeared in the results in [4] which could explain the transient effects at constant input power which the authors reported. Because this anomaly under vacuum conditions always appeared at temperatures above 1000°C, it was decided to only report measured emissivities up to 1000°C as shown in the following figures. The emissivity would only increase with further increasing temperature.

Figure 6 shows the emissivity vs. surface temperature for the Inconel in as rolled conditions. The

results indicate a moderately low emissivity which increases from a value of approximately 0.20 at a surface temperature of 200°C to 0.33 at a temperature of 1000°C.

Figures 7a-c show the emissivity vs. surface temperature curves for an oxidizing surface temperature of 1000°C. Several phenomena can be can be seen from these data: oxidation increases the emissivity by a significant amount as was noted earlier (Fig. 1) and is evident by comparing Figs. 7a-c with Fig. 6. Also, there is an appreciable increase of emissivity with surface temperature.

Figure 8 plots the data of Figs. 7a-c on a single graph where it is easier to examine the effect of oxidation time. From Fig. 8, the 30-minute oxidation sample has a lower emissivity than the 15-minute sample. On the other hand, the 60-minute sample has a greater emissivity than the other two. Thus, at least for these data (oxidized at 1000°C), there does not seem to be a simple relation between emissivity and oxidation time. This same result will again be apparent in the discussions of the tests which were pre-oxidized at 1100°C and 1142°C.

Figures 9a-c present the surface temperature vs. emissivity data for the case of pre-oxidation at a surface temperature of 1100°C. There are some striking differences between these data and those for which the oxidation occurred at a surface temperature of 1000°C (Figs. 7a-c). For the low temperature emissivity measurements (200°C T_{SUR} 800°C) the emissivities for samples with 1000°C oxidation temperatures are significantly lower than the emissivities for samples with 1100°C oxidation temperatures. For example, at a surface temperature of 300°C, the 15 minute-1100°C oxidation temperature emissivity is approximately equal to 0.85 while for the 15 minute-1000°C

oxidation temperature, the emissivity is equal to 0.65, a decrease of 31%. Thus, the oxidation temperature has a significant influence on the emissivity in the low temperature range.

It will also be noted in examining Figs. 9a-c that emissivity measurements were made with both ascending and descending surface temperatures. For oxidation times of 15 and 30 minutes, both ascending and descending data show reasonable agreement. However, for the oxidation time of 60 minutes the descending data are lower than the ascending data. One possible explanation for this behavior is that the thicker oxidized layer at the higher oxidation time is more sensitive to surface spalling as the surface area expands and contracts with temperature. Although the thermal expansion area change was accounted for in the emissivity calculations, it was not possible to visually examine the oxidized surface conditions for spalling while the surface area was changing with temperature. However, some black powdery oxide was found in the vacuum chamber after the tests which supports this contention. As the sample length and width dimensions change with temperature from 200°C to 1000°C, the linear dimensions of the samples are calculated to increase by approximately 1.3%.

Figures 10a-c present the emissivity vs. temperature data for the case of pre-oxidation at a temperature of 1142°C. In general, the emissivity vs. temperature data approximately agree with the data for an oxidation temperature of 1100°C. Also, once again as seen in Fig. 9c, the descending data for an oxidation time of 60 minutes are lower than the ascending data as was the case for the oxidation temperature of 1100°C.

Table 5 presents the maximum measured emissivities for each of the experiments as a function of the

pre test oxidation times and temperatures. These maxima in the emissivity were chosen from the experimental data for each experiment over the test temperature range up to 1000°C and are, as a rule, the measured emissivities at 1000°C. It is evident from the table that the sample emissivity increases with pre test oxidation temperature from 1000°C to 1100°C, but that there is little additional increase, if any, as the pre test oxidation temperature increases to 1142°C. There is no apparent trend in the emissivities as the time of pre-oxidation is varied from 15 minutes to 60 minutes. This is fortunate in so far as application of the test results to a heat transfer transient does not appear to involve a significant transient in the emissivity itself.

6. PRACTICAL SIGNIFICANCE

The performance of systems at elevated temperatures frequently relies on the ability of thermal radiative heat transfer to reject heat from the system when other heat transfer mechanisms become ineffective. The system's ability to function normally at elevated temperatures or to recover from transient off-normal conditions will usually depend upon not exceeding some threshold temperature, usually determined by some material property or other failure criteria. This can be the case for materials used in transportation systems, accelerator target systems, nuclear reactor components, materials for space applications, compact power generation systems, among others, in which the system is either required to operate at elevated temperatures or may experience such conditions undesirably.

Oxidation of metal components, either intentionally or as the result of a thermal transient in an oxidizing environment, will increase the emissivity of the surfaces, thus improving the heat rejection

capability of the system by thermal radiation to nearby heat sinks. Although most mechanical systems are assembled from polished, metallic components for practical reasons (such as dimensional tolerance, cleanliness, reliability and maintainability), designers may wish to consider pre-oxidation of selected components where enhanced thermal radiation heat transfer performance is desired in order to increase radiative emissivities and thus reduce operating temperatures.

7. CONCLUSIONS

Total hemispherical emissivities were measured for Inconel 718 under a variety of surface temperatures and surface oxidation conditions. The following results were obtained:

1. Unoxidized Inconel 718 in an as received condition had emissivities that increased from approximately 0.24 to 0.33 over a surface temperature range of 200°C to 1000°C.

2. When the surface was oxidized in air at atmospheric pressure with temperatures of 1000°C, 1100°C and 1142°C, the emissivity increased slightly with temperature in the approximate range from 0.85 to 0.90 over the temperature range from 200°C to 1000°C.

3. No conclusive trend of emissivity was observed as a function of oxidation time (15 to 60 minutes) at a given oxidation temperature.

4. Emissivity measurements made at the highest oxidation time at increasing surface temperatures were greater than those repeated at decreasing surface temperatures. One

possible reason for this could be the spalling of the oxide layer as the surface changed its dimensions with temperature. This behavior would be self-correcting in an oxidizing environment while these experiments were, by necessity, performed in a vacuum.

8. RECOMMENDATIONS AND FUTURE RESEARCH NEEDS

This study only considered the thermal radiative emissivities of pre-oxidized Inconel 718 at temperatures up to 1000°C. It is the expectation of the authors that other Inconel alloys will perform qualitatively similarly if pre-oxidized in air, however additional studies with other alloys (i.e., Inconels and stainless steels) would be useful to expand the available data base and to confirm the present trends. In addition, the data reported in this paper were truncated at 1000°C due to the thermocouple anomaly presented in Fig. 5. This study used type-S thermocouples (Pt/Pt-10%Rh) for the measurement of the sample temperatures. The wires were individually spot welded to the polished Inconel 718 strips as close to each other as practical. The temperature anomaly first appeared at 1000°C upon the first temperature ramp through 1000°C; the deviation from the standard calibration thermocouple recovered when the temperature increased to 1200°C. The trend of the deviation repeated itself with repeated thermal cycling as shown in Fig. 5. A systematic study with other thermocouple types, different substrates such as other Inconels and stainless steels, various thermocouple attachment methods (i.e., individually spot welded wires, wires spot welded to each other then spot welded to the surface), and thermal cycling in oxidizing as well as inert atmospheres would be desirable in order to help explain this anomalous behavior and to improve our fundamental understanding of thermocouple behavior under atypical conditions.

NOMENCLATURE

A	surface area (m^2)
e	fractional error (-)
E_b	black body radiation (W/m^2)
F	angle factor (-)
G	irradiation (W/m^2)
i	current (amps)
J	radiosity (W/m^2)
	sample length (m)
Q	radiation heat flow (W)
R	electric resistance (ohms)
V	voltage (volts)
w	sample width (m)
α	absorptivity (-)
Δ	increment (-)
ϵ	emissivity (-)
σ	Stefan-Boltzmann constant ($W/m^2\ K^4$)
ρ	reflectivity (-)

REFERENCES

1. Touloukian, Y. S. and D. P. DeWitt, Thermal Radiative Properties-Metallic Elements and Alloys, v. 7 in the TPRC series, Thermophysical Properties of Matter, Plenum Publishing Corporation (1970).
2. Nuclear Systems Materials Handbook, TID-26666; Book 1, Part 1, Group 4, Section 5: Alloy-718, Thermal Emissivity (Stably Oxidized).
3. DeCorso, M. S. and R. L. Colt, Measurement of Total Emissivities of Gas-Turbine Combuster Materials, ASME Paper No. 54-SA-26 (1954).
4. Richmond, J. C. and W. N. Harrison, Equipment and Procedures for Evaluation of Total Hemispherical Emittance, Am. Ceramic Soc. Bull., 39(11), pp. 668-673 (1960).
5. Funai, A. I., A Multichamber Calorimeter for High Temperature Emittance Studies, in Measurement of Thermal Radiation Properties of Solids, NASA SP-31, pp. 317-327 (1963).
6. Masuda, H. and M. Higano, Measurement of Total Hemispherical Emissivities of Metal Wires by Using Transient Calorimetric Technique, J. Heat Transfer, 110, pp. 166-172 (1988).
7. Alaruri, S. D., L. Bianchini and A. Brewington, Integrating Sphere Method for Determining the Effective Spectral Emissivity of Superalloys at High Temperatures Using a Single Wavelength Pyrometer, Optical Engineering, 35, pp. 2736-2742 (1996).
8. Brant, J. A., T, F. Irvine, Jr. and E. R. G. Eckert, A Method of Measuring Total Hemispherical Emissivities at Low Temperatures - Results for Pure Iron from 300 to 500 Degrees Rankine, Proceedings of the 1960 Heat Transfer and Fluid Mechanics Institute, Mason, Reynolds and Vincenti, Eds., Stanford University Press, Stanford, California (1960).
9. Carslaw, H. S. and J. C. Jaeger, Conduction of Heat in Solids, 2nd Edition, p. 261, Oxford Science Publications (1986).
10. High Temperature, High Strength Nickel Base Alloys, The International Nickel Company, Inc., 3rd Edition, p. 4 (1977).

LIST OF FIGURES

Figure 1. Variation of total hemispherical emissivity of Inconel with temperature and surface conditions [3]: [A] as rolled and received, [B] as received and oxidized for 15 minutes at 815°C, [C] sandblasted and oxidized for 15 minutes at 815°C.

Figure 2. Radiation between two surfaces where G = Irradiation, J = Radiosity.

Figure 3. Schematic of Inconel 718 sample: x = thermocouple wires.

Figure 4. Schematic of emissivity measurement system: a- Inconel 718 sample, b- enclosure, c- springs, x- thermocouple wires.

Figure 5. Temperature difference between sample thermocouple and reference thermocouple.

Figure 6. Total hemispherical emissivity vs. sample temperature for Inconel 718 (non-oxidized) in as rolled condition.

Figure 7. Total hemispherical emissivity vs. sample temperature for Inconel 718, oxidized at 1000°C for 15 minutes [A], 30 minutes [B], 60 minutes [C].

Figure 8. Comparison of emissivities vs. sample temperature for various oxidation times (oxidized at 1000°C).

Figure 9. Total hemispherical emissivities vs. sample temperature for Inconel 718, oxidized at 1100°C for 15 minutes [A], 30 minutes [B], 60 minutes [C].

Figure 10. Total hemispherical emissivity vs. sample temperature for Inconel 718, oxidized at 1142°C for 15 minutes [A], 30 minutes [B], 60 minutes [C].

LIST OF TABLES

Table 1. Emissivity differences with and without compliance with Kirchhoff's law.

Table 2. Measurement errors in the calculation of emissivity.

Table 3. Constituents of Inconel 718.

Table 4. Run numbers for various pre test oxidation times and temperatures.

Table 5. Maximum emissivities for various pre test oxidation times and temperatures over the test temperature range up to 1000°C.

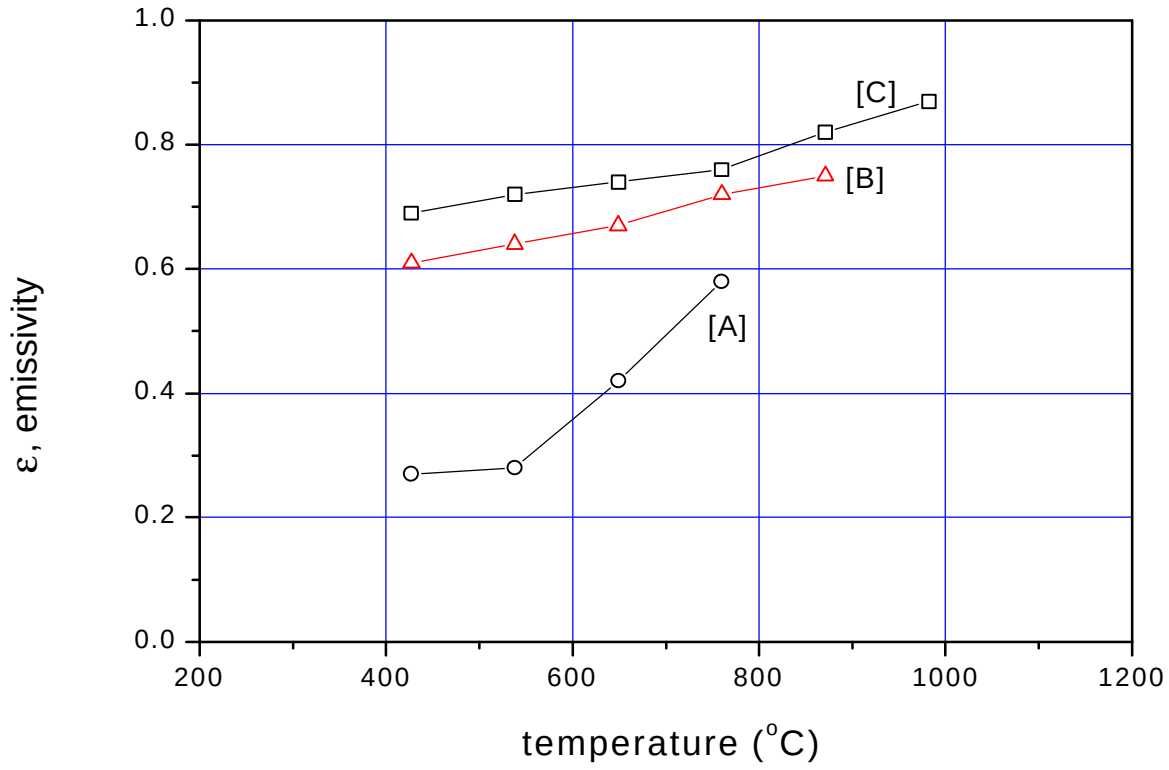

Figure 1. Variation of total hemispherical emissivity of Inconel with temperature and surface conditions [3]: [A] as rolled and received, [B] as received and oxidized for 15 minutes at 815°C, [C] sandblasted and oxidized for 15 minutes at 815°C.

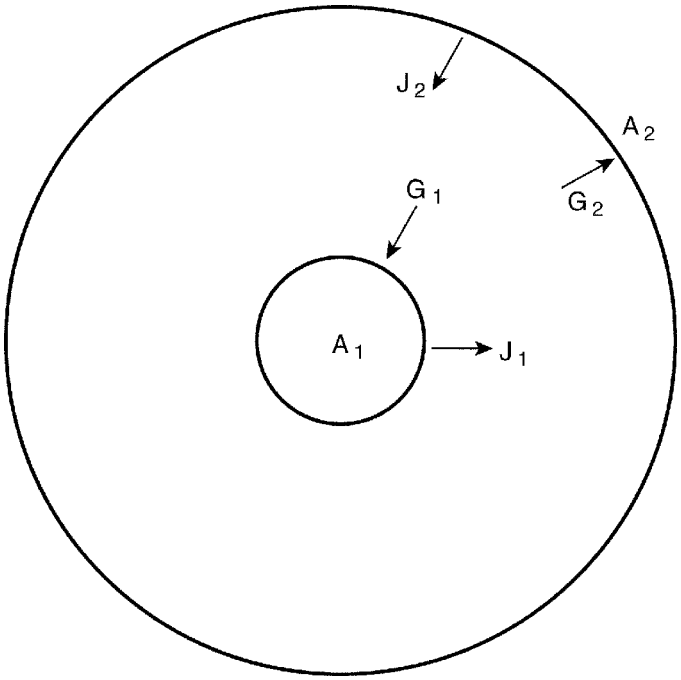

Figure 2. Radiation between two surfaces where G = Irradiation, J = Radiosity.

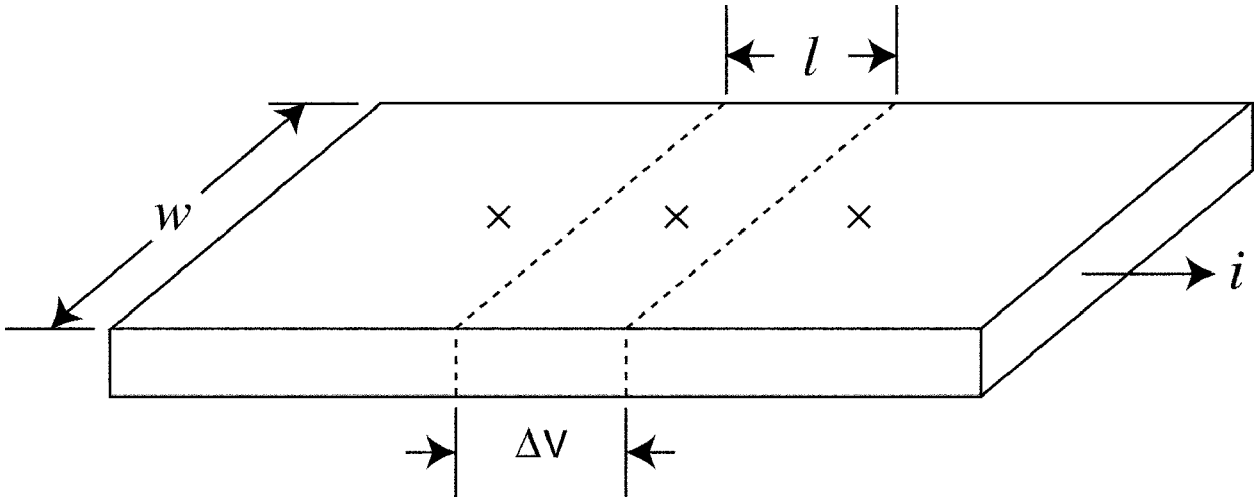

Figure 3. Schematic of Inconel 718 sample: x = thermocouple wires.

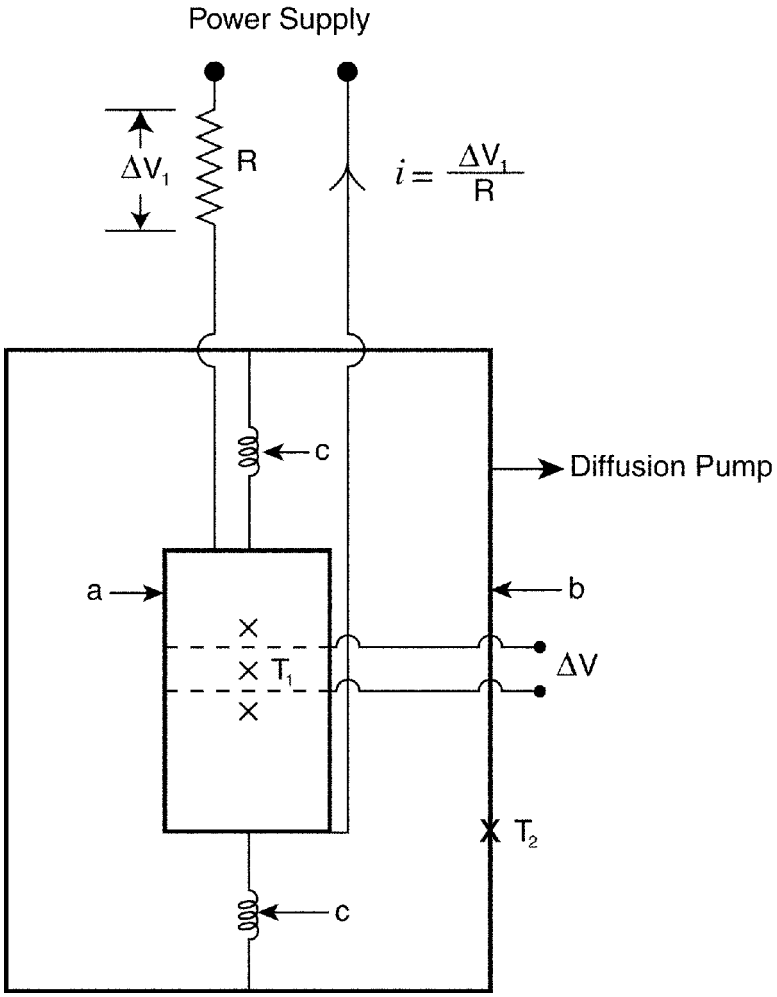

Figure 4. Schematic of emissivity measurement system: a- Inconel 718 sample, b- enclosure, c- springs, x- thermocouple wires.

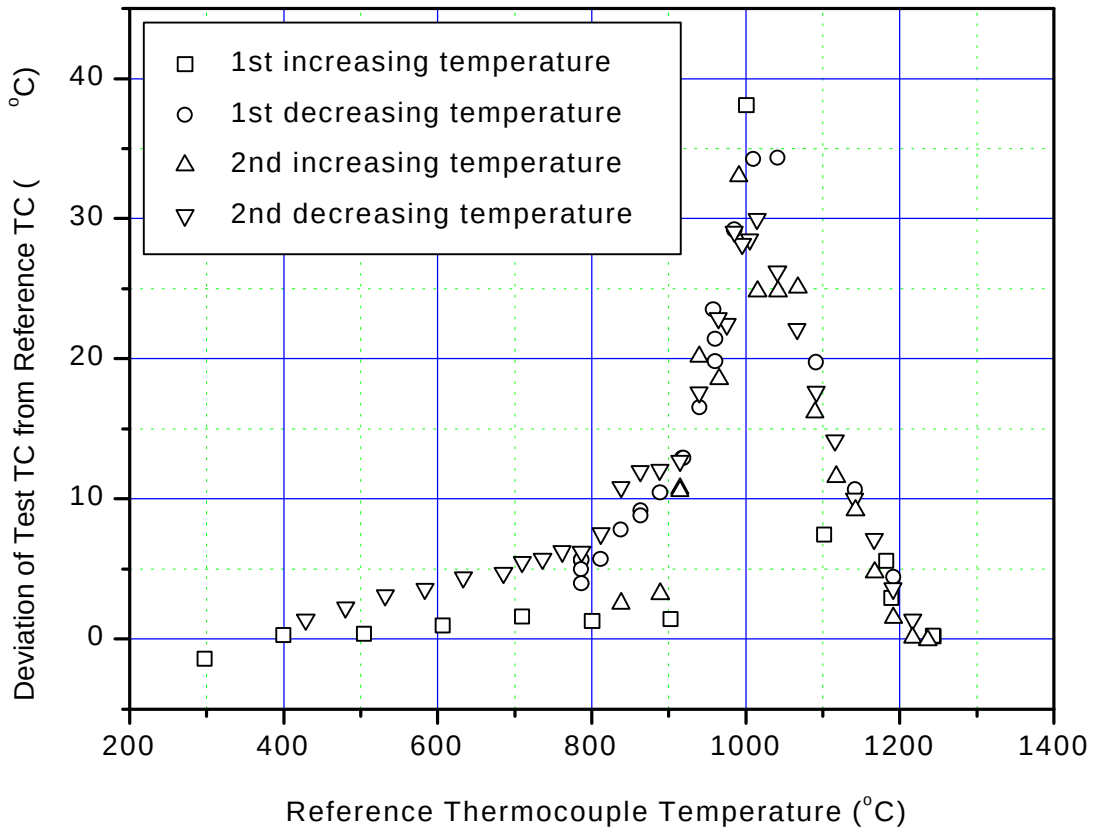

Figure 5. Temperature difference between sample thermocouple and reference thermocouple.

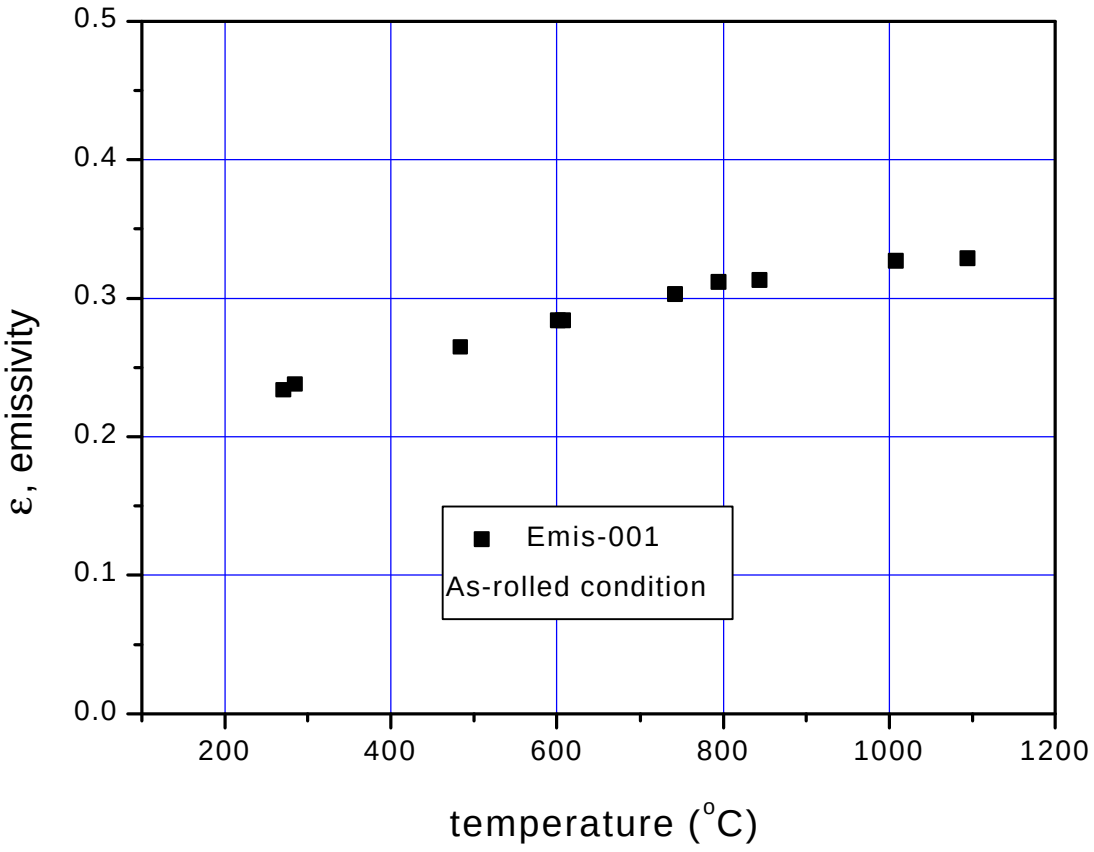

Figure 6. Total hemispherical emissivity vs. sample temperature for Inconel 718 (non-oxidized) in as rolled condition.

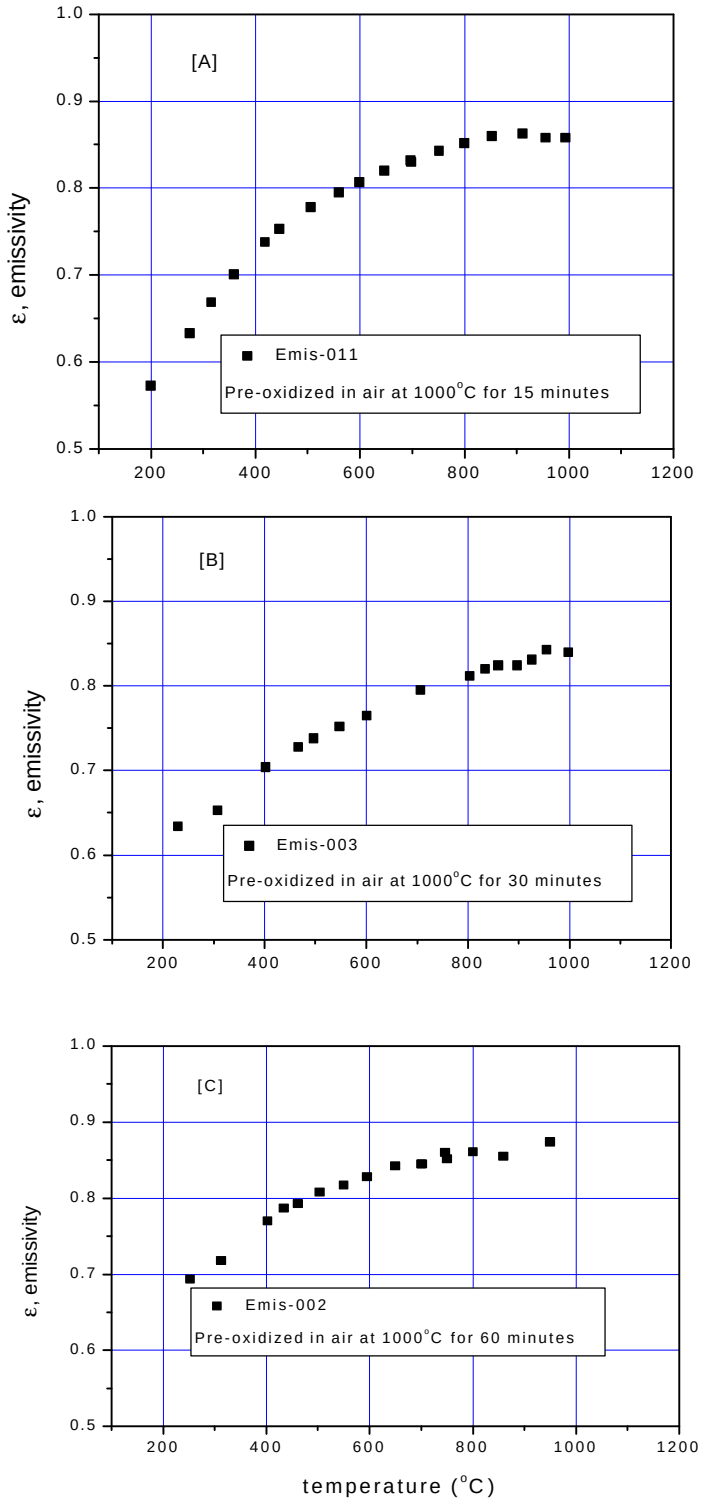

Figure 7. Total hemispherical emissivity vs. sample temperature for Inconel 718 oxidized at 1000°C for 15 minutes [A], 30 minutes [B], 60 minutes [C].

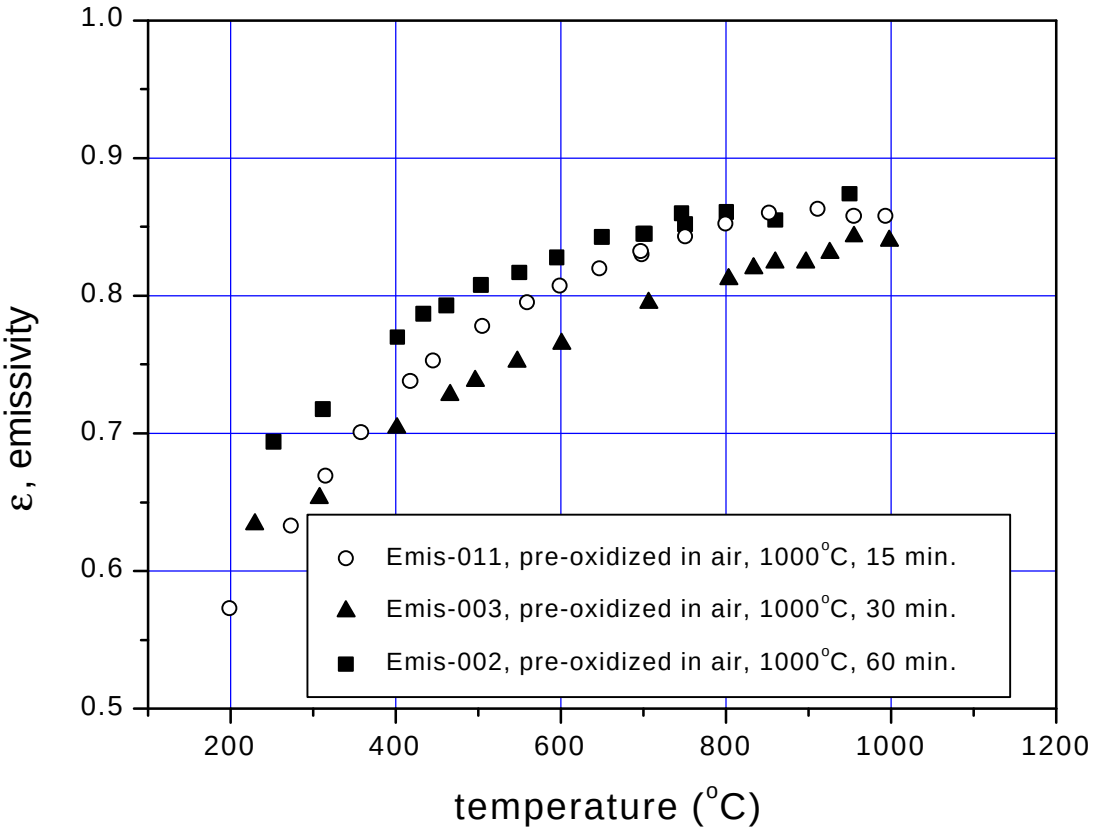

Figure 8. Comparison of emissivities vs. sample temperature for various oxidation times (oxidized at 1000°C).

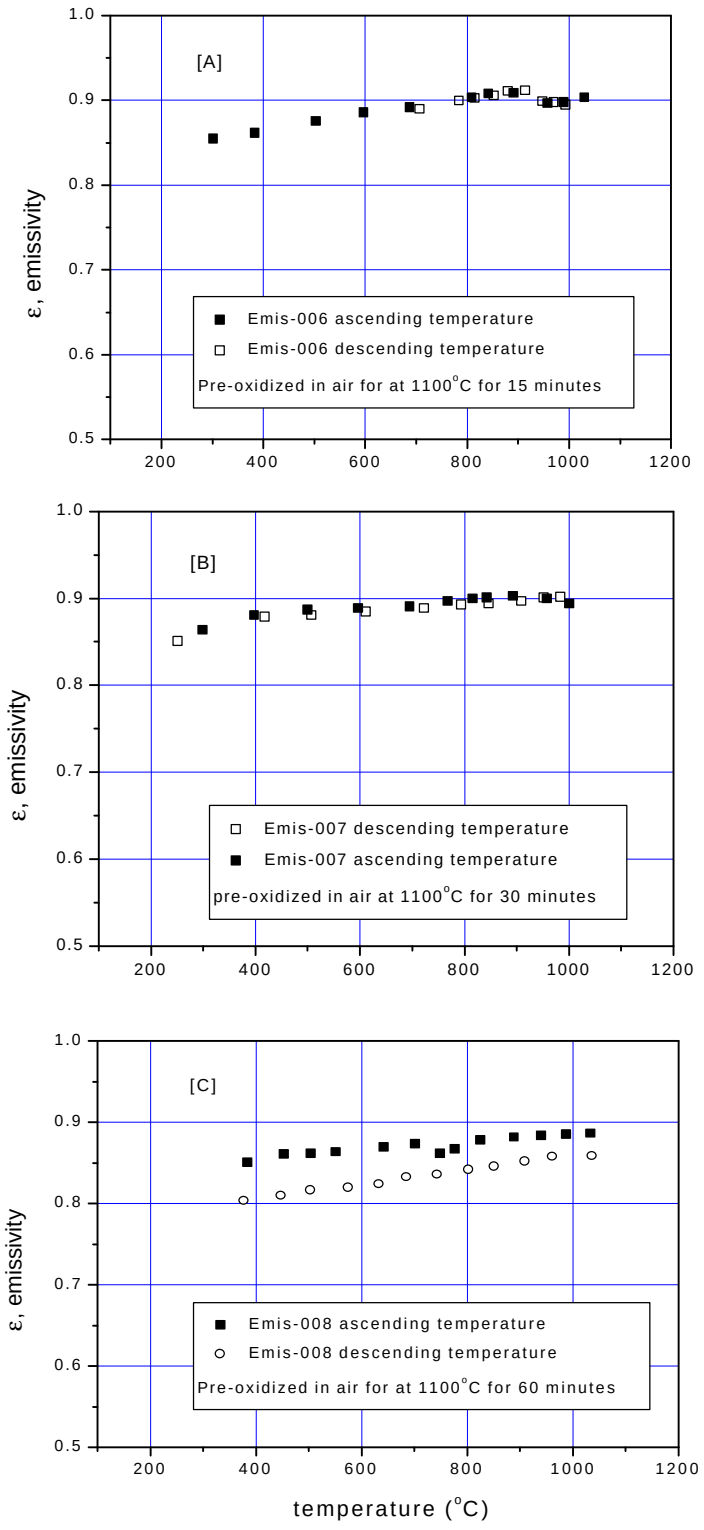

Figure 9. Total hemispherical emissivity vs. sample temperature for Inconel 718 oxidized at 1100°C for 15 minutes [A], 30 minutes [B], 60 minutes [C].

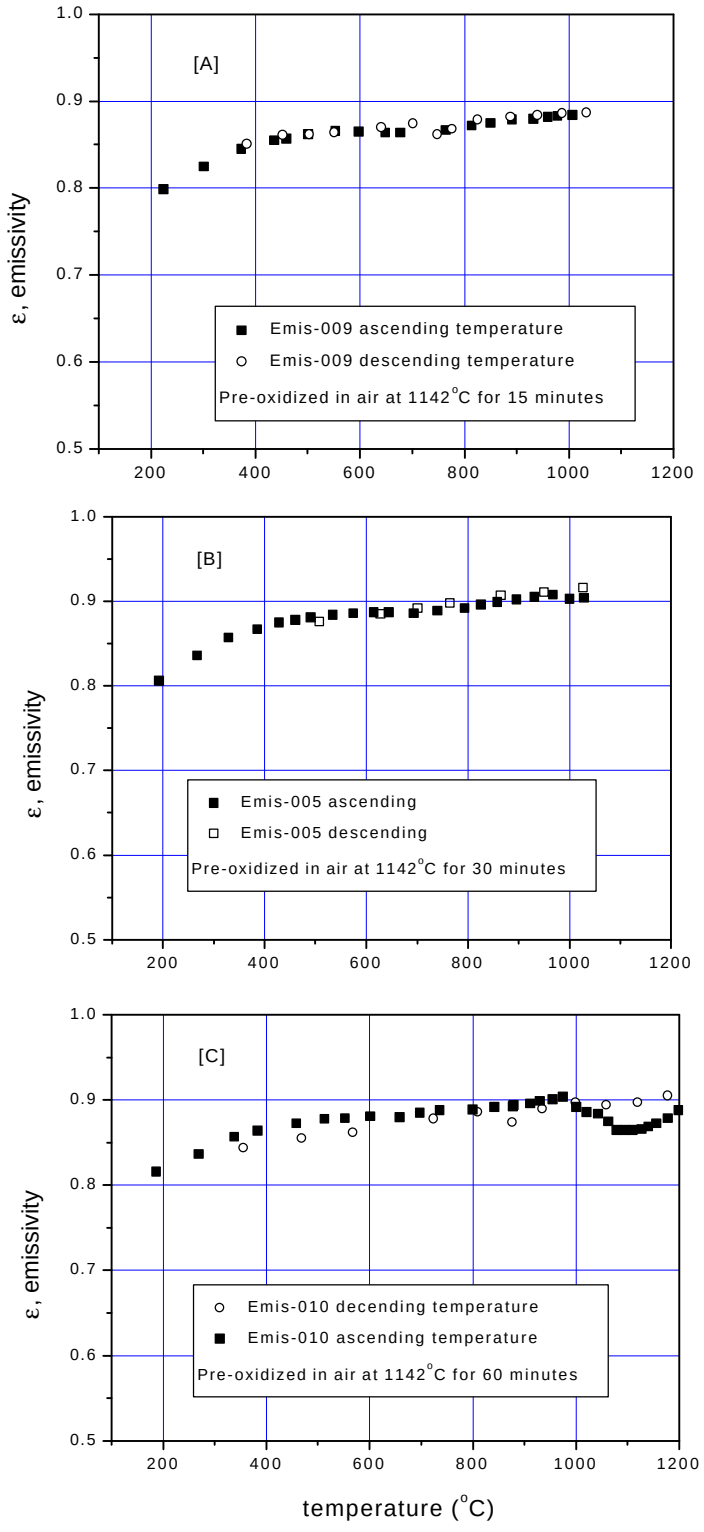

Figure 10. T otal hemispherical emissivity vs. sample temperature for Inconel 718 oxidized at 1142 °C for 15 minutes [A], 30 minutes [B], 60 minutes [C].

Table 1

Emissivity differences with and without compliance with Kirchhoff's law

T_1 (K)	Difference (%)
573	7.5
673	3.9
773	2.3
823	1.8
873	1.4
973	0.9
1073	0.6
1173	0.4
1273	0.3

Table 2

Measurement errors in the calculation of emissivity

Independent Variable	Measurement Range	Measurement Uncertainty	Fractional Error
Current, i	50 mV	± [0.04 % + 400μV]	0.0084
Voltage drop, ΔV	1 V	± [0.04 % + 4 mV]	0.0044
Sample length, ℓ	1 inch	± 0.0005 inch	0.0005
Sample width, w	0.1 inch	± 0.0001 inch	0.0010
Sample temperature, T_1	1000 K	calculated, $4\Delta T_1/T_1$	0.0170
Enclosure temperature, T_2	300 K	calculated, $4\Delta T_2/T_2$	0.0130
Emissivity, ϵ	0.6 - 0.9	RMS error	0.0234

Table 3

Constituents of Inconel 718 [10]

Constituent	% of Weight
Ni	52.5
Cr	19.0
Fe	18.5
Nb	5.2
Mo	3.0
Ti	0.8
Al	0.6
Si	0.2
Mn	0.2

Table 4

Run numbers for various pre test oxidation times and temperatures

Oxidation Times (minutes)	Oxidation Temperature (°C)		
	1000	1100	1142
15	011	006	009
30	003	007	005
60	002	008	010

Table 5

Maximum emissivities for various pre test oxidation times and temperatures* over the test temperature range up to 1000°C

Oxidation Times (minutes)	Oxidation Temperature (°C)		
	1000	1100	1142
15	0.86	0.90	0.89
30	0.84	0.90	0.91
60	0.88	0.89	0.91

*The peak emissivity for the non-oxidized sample was 0.33.